Geomechanics and Engineering, *Vol. 18, No. 1 (2019) 71-83*
DOI: https://doi.org/10.12989/gae.2019.18.1.071

Creep-permeability behavior of sandstone considering thermal-damage

Bo Hu[a], Sheng-Qi Yang* and Wen-Ling Tian[b]

State Key Laboratory for Geomechanics and Deep Underground Engineering, School of Mechanics and Civil Engineering, China University of Mining and Technology, Xuzhou 221116, P.R. China

(Received March 6, 2019, Revised April 15, 2019, Accepted April 24, 2019)

Abstract. This investigation presented conventional triaxial and creep-permeability tests on sandstones considering thermally-induced damage (TID). The TID had no visible effects on rock surface color, effective porosity and permeability below 300°C TID level. The permeability enlarged approximately two orders of magnitude as TID increased to 1000°C level. TID of 700°C level was a threshold where the influence of TID on the normalized mass and volume of the specimen can be divided into two linear phases. Moreover, no prominent variations in the deformation moduli and peak strength and strain appeared as TID<500°C level. It is interesting that the peak strength increased by 24.3% at 700°C level but decreased by 11.5% at 1000°C level. The time-related deformation and steady-state creep rate had positive correlations with creep loading and the TID level, whereas the instantaneous modulus showed the opposite. The strain rates under creep failure stresses raised 1-4 orders of magnitude than those at low-stress levels. The permeability was not only dependent on the TID level but also dependent on creep deformation. The TID resulted in large deformation and complexity of failure pattern for the sandstone.

Keywords: thermally-induced damage; sandstone; physical changes; creep behavior; permeability

1. Introduction

The physical and mechanical parameters of rock on the action of temperature-damage are essential references for designing rock engineering projects. In deep excavations, high-temperature and high geo-stress bring great challenges for rock mechanics researchers (Moradi *et al*. 2018). Therefore, research on the mechanical response of rock considering the TID effect becomes a science problem and brings a vital research direction in geo-engineering, deep mining (Lyons *et al*. 2007, Zhang *et al*. 2015), radioactive nuclear waste disposal (Miura *et al*. 2003), geothermal resource development (Tiskatine *et al*. 2016, Kumari *et al*. 2017), underground coal gasification (Minchener 2005, Ranjith *et al*. 2012, Otto and Kempka 2015) and thermal viscous oil production (Shafiei and Dusseault 2013, Uribe-Patiño *et al*. 2017), etc.

The most intuitive effect of temperature on rocks is the change in physical properties. Rock mass, volume, density and surface color (Tian *et al*. 2012, Zhang *et al*. 2016, Sun *et al*. 2016), porosity (Tian *et al*. 2012, Sun *et al*. 2017), wave velocity (David *et al*. 1999, Sun *et al*. 2017), thermal conductivity and diffusivity (Tang *et al*. 2015, Sun *et al*. 2016), permeability (Géraud 1994, Tian *et al*. 2012, Zhang *et al*. 2016) and mineral components (Somerton 1992, Hajpál and Török Á 2004, Liu *et al*. 2016) showed apparent temperature dependence. The variations in the physical characteristic will ultimately result in the changes in mechanical characteristic of rock.

During the heating process, mineral grains thermally expanded generating extra inner stresses acting on the boundary of the grains. This local stress concentration is prone to promote the development of micro-cracks between grains. As temperature cooling down to room temperature, some permanent changes cannot recover. As a result, the accumulated TID deteriorated the rock loading capacity (David 1999). However, this can also elevate the rock strength (Luo and Wang 2011). The mechanism of the TID effect within rock was very complex (Heuze 1983, Scott and Nielsen 1991, Hudson *et al*. 2005, Chen *et al*. 2017a). Plenty of uniaxial and conventional triaxial compression experiments were conducted on various rocks by researchers. The effect of temperature on sandstone deformability parameters including elastic modulus, Poisson's ratio and characteristic stresses (i.e., crack closure stress, initiation stress, crack damage threshold, peak stress, residual stress and tensile strength) as well as strength parameters (i.e., cohesion, friction angle, H-B parameters: m and s) were obtained from the tests (Ranjith *et al*. 2012, Zhang *et al*. 2016, Gautam *et al*. 2016, Yang *et al*. 2017, Lü *et al*. 2017, Huang *et al*. 2017, Wu *et al*. 2019). However, the quantitative relationships between temperature and the mechanical parameters of sandstone are not identical which is dependent on the sandstone property.

Moreover, the TID effects should be considered for long-term safety evaluation during the rock engineering service. Chopra (1997) conducted high temperature creep experiments to research the creep properties of the dunites and then simulated the time-dependent deformation. Heap *et al*. (2009) reported that under triaxial compression, the resistance and creep deformation of the tested sandstone

*Corresponding author, Professor
E-mail: yangsqi@hotmail.com
[a]Ph.D.
E-mail: huboskl@hotmail.com
[b]Ph.D.
E-mail: tianwenling3@163.com

http://www.techno-press.org/?journal=gae&subpage=7
ISSN: 2005-307X (Print), 2092-6219 (Online)

were affected by temperature. Ye *et al*. (2015) reported that the deformation relating creep of green tuff showed an apparent temperature-dependence. Chen *et al*. (2017b) found that temperature existed a prominent effect on granite creeping deformation. The time-dependent behaviors and long-term permeability evolution of surrounding rocks are vital features for the deep underground excavations design and evaluation. However, there have few investigations on the creep-permeability behavior of sandstone considering thermal-damage.

The objective of this laboratory investigation is to build quantitative correlations of the mechanical parameters and TID level as well as increases the understanding of creep-permeability of sandstone considering TID which will help for the long-term stability design for underground excavation. This work performed triaxial compression under constant strain rate and constant stress loadings at constant confinement on the sandstones. The compression strength, deformational responses and failure types of the specimen on action of the TID were researched. The creep response, time-based rupture pattern, and creep-permeability behaviors of the TID sandstones were also analyzed in this research. Moreover, microscopic observation method was adopted to detail the mechanism of the TID effects on the microstructure, deformation, and permeability of the tested specimens.

2. Experimental materials and methodology

2.1 Rock specimens

All the researched sandstones, showing homogeneous and high-level hard, were drilled from Rizhao, Shandong province in China. The primary mineral composition in the sandstone includes feldspar, quartz, debris, and cement (Yang *et al*. 2014). They were cored and polished on cylindrical samples (50×100 mm) based on the suggested method by ISRM (2007). Six levels of TID, i.e., 25, 300, 500, 700, 900 and 1000°C, were set using a heating furnace. To avoid the influence of temperature gradient, a heating rate of 5°C per minute was selected. The samples were cooling down to ambient temperature after holding target temperatures for 2 hours. The experimental information of the tested sandstone is presented in Table 1.

2.2 Testing apparatus

A rock triaxial facility (Fig. 1) was utilized to perform the conventional loading (at a constant strain rate) and creep loading (at constant stresses) tests on the sandstones with different TID levels. This apparatus has independent deviatoric, hydrostatic and pore pressure loading systems. Constant-stability pressure system can maintain the applied constant stresses. Furthermore, the inlet and outlet pump can regulate the water pressures in upstream and downstream reservoirs, respectively. A pressure-reducing valve was employed to control the injected gas pressure. This facility can provide two test conditions—constant volume and constant fluid pressure. The former one was selected to measure the gas permeability during creep compression.

Table 1 Measured specimen's geometry and physical properties after different temperature tested through conventional and creep loading

T (°C)	Length (mm)	Diameter (mm)	Mass (g)	Density(kg/m^3)	Porosity (%)	Loading type
25	101.25	50.20	481.3	2401.7	6.26	Conventional loading
300	100.23	50.32	475.1	2383.5	5.74	
500	100.45	50.35	470.8	2353.9	7.79	
700	98.55	50.50	459.9	2329.9	7.59	
900	101.20	51.00	467.0	2258.9	11.86	
1000	101.35	50.18	466.3	2326.4	13.09	
25	99.46	50.30	473.4	2395.3	6.55	Creep loading
300	100.47	50.30	484.0	2411.0	6.10	
700	99.94	50.46	470.4	2437.2	9.14	
1000	101.97	51.15	469.6	2409.3	13.37	

(a) Test equipment

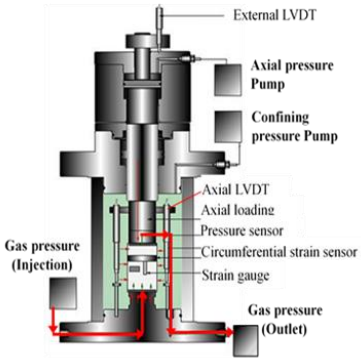

(b) Triaxial cell

Fig. 1 Rock triaxial rheological testing device (modified from Yang *et al*. 2014)

2.3 Testing procedure

To simulate high geo-stress state (i.e., approximately 1000 m depth), the samples were subjected to $\sigma_1=\sigma_2=\sigma_3=25$ MPa compression. Conventional compression at constant strain rate (0.02 mm/min) was first conducted to obtain the peak strength of the sandstone. The applied constant stresses in creep compression were designed referring to the values of peak stress. The tested sample was encased by a nitrile rubber jacket to isolate hydraulic oil. Creep-permeability behaviors of the thermally-damaged sandstones were compared with the mechanical responses of sandstones under conventional loading. Each constant

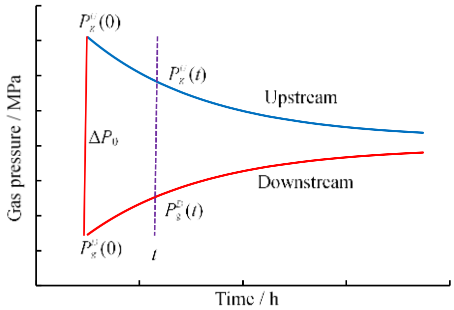

Fig. 2 Time–gas pressure variation diagram of specimen Up- and Down-stream in the Pulse decay method

stress step was last 3.5 to 4 days until accelerating creep occurred. The average value of two parallel axial displacement transformers was used to calculate the axial displacement of rock, and a circumferential displacement transducer was used to record its lateral dilation.

Brace method (Brace *et al*. 1968) is suited for the rock with low permeability. So, this method was used to measure permeability during creep, and inert nitrogen was selected as a flow medium. Fig. 2 shows the schematic diagram of the pulse decay method under constant volume condition.

Inert nitrogen whose viscosity parameter is represented using μ was selected as flow medium. A gas pressure reducing valve was installed at upstream to control the input gas pressure. First, saturating the tested sample under 3 MPa equilibrium pressure where the inlet pressure ($P^U{}_{g(t)}$) equals to that of the outlet gas pressure ($P^D{}_{g(t)}$). Then, closing the inlet pressure and the valve between the inlet and outlet reservoir and forming a gas pressure drop (ΔP_0=0.3 MPa) between inlet and outlet storage reservoirs at t_0. At this moment, the gas pressure in upstream equals $P^U{}_{g(0)}$ and $P^D{}_{g(0)}$ is the pressure in downstream. The unit pressure volumes in inlet and outlet storage reservoirs are α^U and α^D, respectively. Based on the rock height (H) and cross-section area (S), the permeability (k) can be calculated using the Brace method, whose calculation equations are listed as the following equations.

$$P_g^U(t) = P_g^U(0) - \Delta P_0 \cdot \frac{\alpha^U}{\alpha^U + \alpha^D} \cdot (1 - e^{-\frac{\alpha^U + \alpha^D}{\alpha^U \cdot \alpha^D} \cdot \frac{k \cdot S}{\mu \cdot H} \cdot t}) \tag{1}$$

$$P_g^D(t) = P_g^D(0) + \Delta P_0 \cdot \frac{\alpha^U}{\alpha^U + \alpha^D} \cdot (1 - e^{-\frac{\alpha^U + \alpha^D}{\alpha^U \cdot \alpha^D} \cdot \frac{k \cdot S}{\mu \cdot H} \cdot t}) \tag{2}$$

$$k = \frac{\alpha^U \cdot \alpha^D}{\alpha^U + \alpha^D} \cdot \frac{\mu \cdot H}{S} \cdot \frac{\ln \frac{\Delta P(t)}{\Delta P(t + \Delta t)}}{\Delta t} \tag{3}$$

3. Rock specimens physical test results

3.1 Rock color and thermally-induced cracks

The most visualized effect of temperature on the rock is the changes of physical features, such as surface color, mass (M), height (H), diameter (D), volume (V) and effective porosity (p_0) and so on. So, these values were measured before and after high-temperature treatments. Moreover, to

(a) Sandstone samples after heating for conventional loading tests

(b) Sandstone samples after heating for creep loading tests

Fig. 3 View of the heated sandstone specimens with different colors representing the TID levels

explore the microscopic mechanism of the thermal-damage, scanning electron method (SEM) was used to observe micro-cracks within the rock.

The surface color of the specimens subjected to various TID levels (in Fig. 3) were significantly different, varying from gray red to brick red as the TID level increased gradually. Sun *et al*. (2017) also observed a similar phenomenon on red sandstone, and he explained the result from the view of the siderite phase transformation. The temperature dependence of rock color was substantially dependent on the mineralogical composition (Hajpál and Török 2004). Clay minerals and hematite appeared in the red sandstone except for quartz and feldspar (Sun *et al*. 2017). The composition of hematite played a critical role in the change in surface color (Yang *et al*. 2018a).

Fig. 4 plots the SEM observation results. No obvious pre-existing micro-cracks can be observed within the specimens with 25 and 300°C TID levels (Figs. 4(a)-4(d)). Mineral grains and cementation minerals between grains and marginally loose particles expanded commonly due to temperature changed from 25 to 300°C. This thermal-expansion led to the specimens become denser, and there was no obvious crack. When the TID level increased to 700°C, some minerals had been melt or been decomposed (Somerton 1992), boundary cracks and thermally-induced micro cracks in grains can be observed in Figs. 4(e) and 4(f). New micro-cracks initiated and formed within the specimen comparing with the results of the low TID levels. After 1000°C heating, numbers of cracks induced by the TID appeared as shown in Figs. 4(g) and 4(h). The distance between grains was increased due to components thermally expand, which enlarges the rock volume extensively. The TID level increased gradually.

3.2 Effective porosity

Change in the porosity of rock can directly demonstrate the variation in rock permeability. So, according to the suggested method (NSCGPRC 2009), the effective porosity (p_0) of the sample was examined. Fig. 5 summarizes some

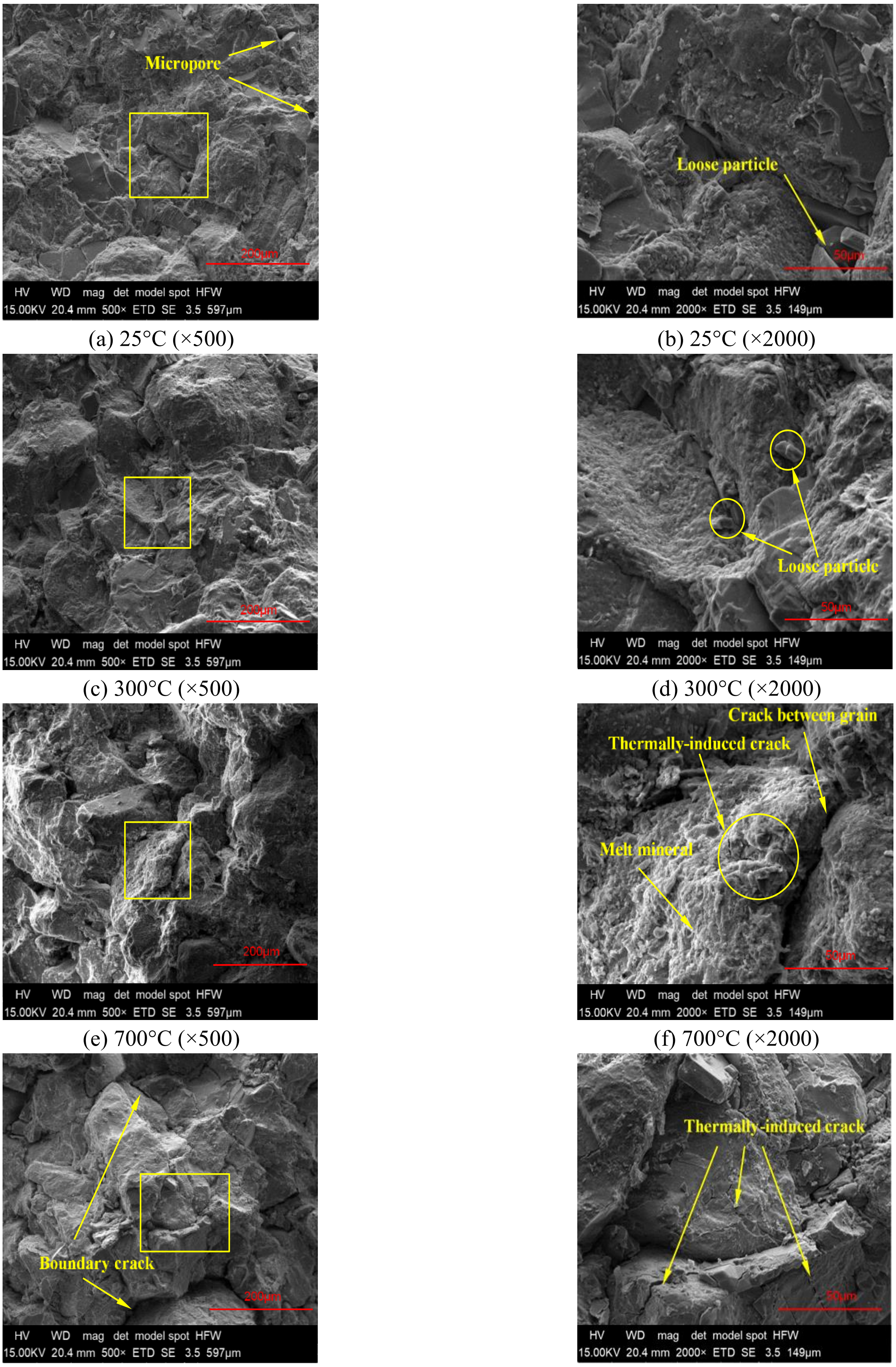

(a) 25°C (×500) (b) 25°C (×2000)

(c) 300°C (×500) (d) 300°C (×2000)

(e) 700°C (×500) (f) 700°C (×2000)

(g) 1000°C (×500) (h) 1000°C (×2000)

Fig. 4 SEM view of the micro-crack evolution at different temperatures

results of the correlations between temperature and the porosity of sandstones. A slight reduction in the p_0 appeared when the TID level reached 300°C. A considerable increase in the p_0 occurred as the TID raised to 1000°C level. The porosity demonstrated a positive correlation with temperature (Sun *et al*. 2016). However, based on the tests results of the rock materials at high-temperature and after heating, the rock porosity had a sudden drop at T=200°C (Sirdesai *et al*. 2017). The initial micro-pores and pre-existing micro-cracks were narrowed due to thermally

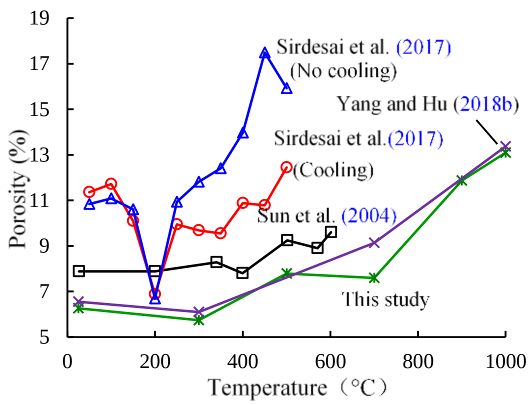

Fig. 5 Temperature–porosity variation of the current test results compared with other researcher results

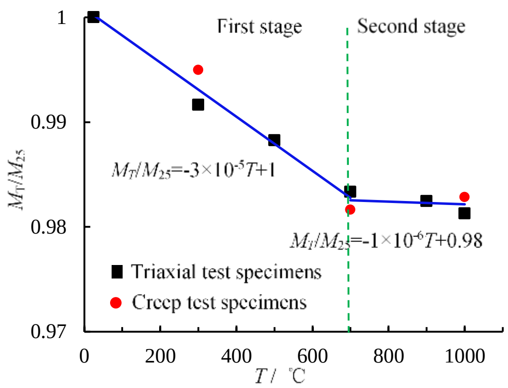

(a) Normalized mass

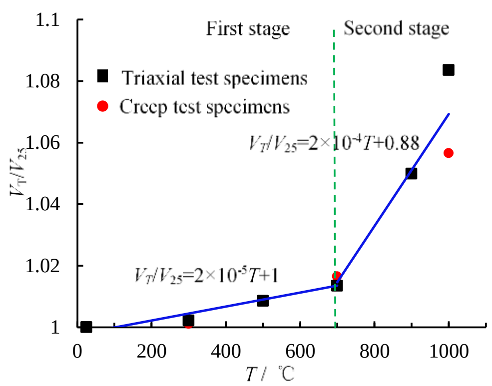

(b) Normalized volume

Fig. 6 Variations of the mass and volume of sandstones under different temperature treatments

expanding. However, porosity continually increased after that temperature. It is complicated for the relationship between the TID and porosity. It varies from rock to rock. So the porosity should consider the TID effect. Moreover, the sample with no TID and the sample with 300°C-TID showed an unobvious difference in the p_0. It is difficult to distinguish whether the TID effect or heterogeneity mainly affects the porosity.

3.3 Mass and volume

The normalized mass (NM) and volume (NV) of rock can be calculated to demonstrate the variations in the M and V affected by the TID. The effects of the TID on the M and V are summarized in Fig. 6. The NM declined considerably when the TID raised to 700°C level, whereas the TID did not affect the NM beyond 700°C. In contrast, the NV showed the opposite trend. A threshold at about 700°C can be identified and the relationships between the TID and the NV and the NM can be divided into two linear stages. The free- and bound-water would evaporate when the temperature ascended to 100-300°C. The TID accumulated within rock that can't be recovered although grains would shrink when cooling (Sirdesai *et al.* 2017). The TID resulted in the mineral grains thermally expanding and increasing the volume of rock. The decomposition of the clay-minerals would occur as the damage increased to 400-700°C-TID and the carbonate minerals in specimen changed above 450°C (Hajpál and Török 2004). When the TID level reached nearly 573°C, the quartz transformed from α to β state (Glover *et al.* 1995), which leads to rock expand and produce micro-cracks. As the TID level increased above 700°C, the calcite would be decomposed (Somerton 1992). The variation in the mass loss was almost unchanged beyond 900°C. As a result, the slope of the NM curve before 700°C was larger than that after 700°C treatment but the NV showed a reverse trend.

4. Triaxial compression and creep-permeability test results

4.1 Time-independent deformation and peak strength

The results of axial strain-deviatoric stress and volumetric strain-deviatoric stress responses of the sandstone with six TID levels are illustrated in Fig. 7. From Fig. 7, two plausible phases can be distinguished (25 < TID < 500 and TID > 500) according to the slopes of the curves.

In phase 1: The strain-stress curves included elastic, yielding, strain-softening and residual deformation stages and there was no distinct densification stage. In this phase, rocks had high stiffness. There was no apparent difference in the slope at elasticity stage. When yield stress was applied, stress-drop before the peak strength occurred. The TID level is higher, the peak strength is larger. In this phase, the closure of the preexisting flaws and pores induced by the thermal expansion led to the rock become denser. So there was no sufficient space to be compacted, showing no compaction stage. The evaporation of water in minerals elevated the frictional resistance between mineral grains, strengthening the loading capacity of minerals and raising the peak strength (Gautam *et al.* 2016).

Phase 2: The compression phase became more evident in addition to the other four deformation stages. The higher the temperature, the lower the rock stiffness as compared to that in Phase 1. The peak strength of the sample reached the largest when temperature increased to 700°C. After that, the peak strength declined dramatically with temperature. Young's modulus (E) was gradually deteriorated by the TID. The residual strength of the specimen at this phase was higher than that at Phase 1. In this phase, thermally-induced cracks appeared as shown in Figs. 4(e)-4(h), and

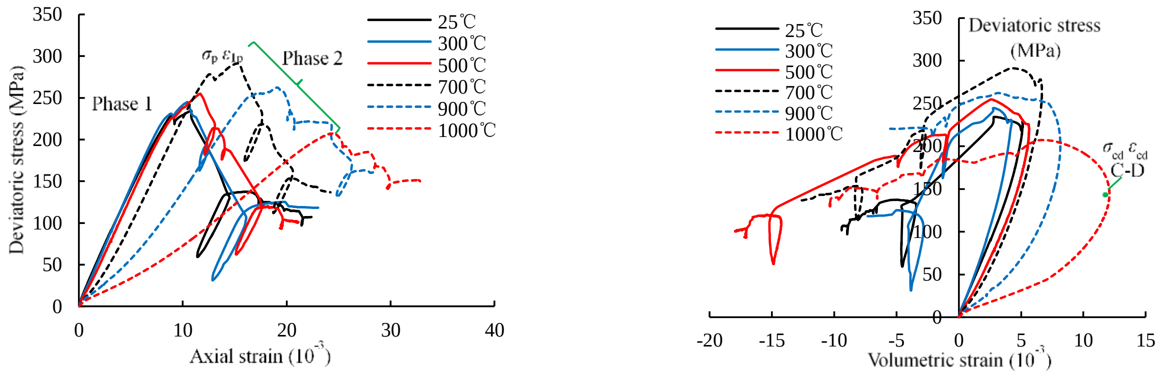

(a) Axial stress-strain (b) Stress-volumetric strain

Fig. 7 Strain-stress curves of the sandstones under different temperature levels

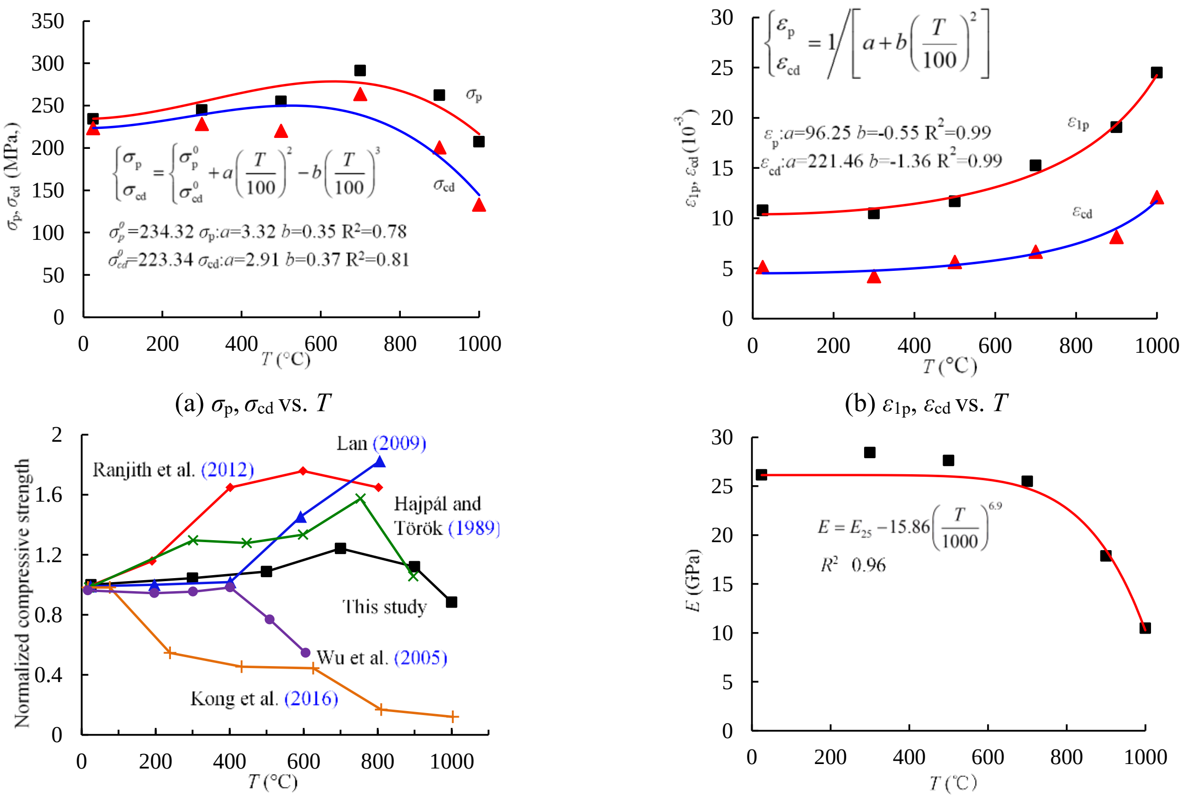

(a) σ_p, σ_{cd} vs. T (b) ε_{1p}, ε_{cd} vs. T

(c) Normalized compressive strength vs. T (d) E vs. T

Fig. 8 Plot of σ_p, σ_{cd} and E as well as ε_{1p} and ε_{cd} vs. temperature of the specimen and relationship between normalized compression strength and temperature

the TID was irreversible. After 700°C heating, although sample thermal-damage occurred, the strength still increased. Under compression, samples were first compacted, thermally-induced cracks were closed, so the compression phase became evident as temperature increased. The residual strength of the specimen beyond 700°C was higher than that at lower temperatures because thermally-induced cracks enhanced the fraction strength between grains and ductile shear became more noticeable (Dragon and Mroz 1978).

According to Fig. 7(b), the volume of the specimen was first compacted, and then dilatation occurred until rupture. The maximum values of stress and strain (i.e., C-D point) in volumetric strain curve denote crack damage stress (σ_{cd}) and crack damage strain threshold ε_{cd}. Table 2 presents the results under constant strain rate loading condition. Figs. 8(a) and (b) plot the relationships between σ_p, σ_{cd}, ε_{1p}, ε_{cd}, and temperature. Both σ_p and σ_{cd} first increased slightly to 700°C and then decreased swiftly beyond 700°C. Two nonlinear fitting equations can predicate their values at different temperatures. Both σ_p and σ_{cd} had no apparent increase below 500°C, whereas exponential growth can be observed after 500°C commonly. Fig. 8(c) also collects some variations in normalized compression strength on the action of temperature. This suggests that thermal-damage exerts complex influence on the strength of the rock. High-temperature may strengthen or deteriorate the rock loading capacity. In Fig. 8(d), the modulus was exacerbated

Table 2 Deformation and strength characteristics of the tested specimens under Pc=25 MPa

T(°C)	TCS (MPa)	σ_{cd} (MPa)	ε_{cd} (10^{-3})	ε_{1p} (10^{-3})	E (GPa)
25	259.32	223.34	5.140	10.788	26.13
300	269.78	228.32	4.247	10.472	28.42
500	279.88	220.25	5.654	11.683	27.60
700	316.29	263.53	6.678	15.262	25.49
900	287.34	200.75	8.148	19.053	17.85
1000	232.36	132.99	12.086	24.478	10.49

*TCS=σ_p+Pc; peak stress: σ_p

Table 3 Sandstones test results under different TID levels during the creep test

T (°C)	σ_p (MPa)	P (MPa)	P/σ_p	ε_{10} (10^{-3})	E_0 (GPa)	Steady-strain rate (h^{-1})	Failure time
25	234.32	160	68%	5.725	27.95	7.146×10^{-4}	
		190	81%	6.956	27.31	1.034×10^{-3}	
		220	94%	8.372	26.28	3.910×10^{-1}	35.3 Min
300	244.78	160	65%	5.958	26.85	7.232×10-4	
		190	78%	7.135	26.23	1.078×10^{-3}	
		220	90%	8.456	26.02	1.427×10^{-3}	
		230	94%	9.024	25.49	6.399×10^{-3}	56.72 h
700	291.29	160	55%	8.047	19.88	7.783×10^{-4}	
		190	65%	9.441	20.12	1.298×10^{-3}	
		220	76%	10.877	20.23	1.577×10^{-3}	
		250	86%	12.889	19.39	6.198	2.5 Min
1000	207.36	160	77%	18.048	8.86	5.905×10^{-3}	
		175	84%	20.805	8.41	8.136×10^{-1}	1.9 h

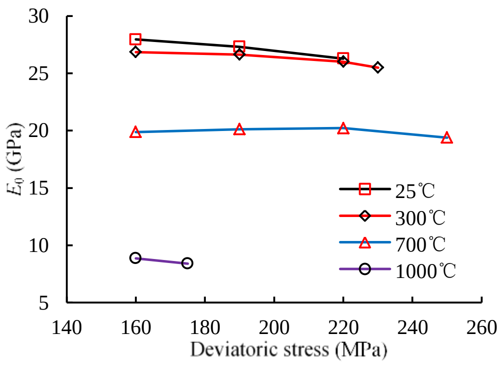

Fig. 9 Relationship between deviatoric stress and instantaneous modulus

gradually as the TID increased where a nonlinear equation can be used to predicate the value of E quantitatively. During the creeping process, the specimens were permitted to deform gradually over time under constant deviatoric stresses until failure. The creep stress levels were applied according to the peak stress of the sample. Gas permeability was measured using transient pulse decay technique during the creeping process. Various instantaneous strains (ε_{10}) and strain rates were yielded under different creep stress levels. The influence of the creep stress on the instant modulus (E_0) and the creep strain rate were also investigated via the long-term tests at a Pc of 25 MPa. Table 3 summarizes all important creep test results.

4.2 Creep deformation

Fig. 9 summarizes the changes in the instantaneous modulus at different creep stress levels. The TID deteriorated E_0 especially after 700°C. The TID is higher, the E_0 is smaller. The E_0 slightly declined as creep stress increased. However, no visible change of the sandstone after 700°C heating can be observed when creep stress was less than 220 MPa.

In Fig. 10, step-like increase in axial strain can be observed under incremental creep stress and time. But the time increasing deformation was less than the stress-induced deformation. Under constant loadings, axial strain increased at a decreasing strain rate that termed as the decelerating creep. Subsequently, a linear increase in axial strain (termed secondary creep) continued until accelerating creep or unloading the applied constant stress. If the applied constant stress levels were sufficiently high, brittle creep failure would occur after the former stage. Specifically, the sample with 300°C-TID appeared tertiary creep after 56.72 hours when applying 230 MPa deviatoric stress. However, the 1000°C specimen deformed abnormally at around 101.3 h during the secondary creep stage. In contrast, high TID level was prone to induce a large axial strain of the sandstone. The deformation of the sandstone after the most top temperature treatment was nearly three times that of the others.

The results of the constant loading tests also showed that the creep deformation behaviors of the specimens were dependent critically on temperature. When the TID level ascended to 1000°C, not only the instant deformation but also the time-dependent deformation became more and more visible under the same stress levels, and the corresponding creep failure stresses gradually decreased from 94% of σ_p to 84% of σ_p. The heterogeneity was one of the natural characteristics of rocks, which means that different load-bearing capability of the material randomly distributed within the rock. Under constant loading condition, the mineral grains generated elastic-viscoplastic deformation and the time-dependent micro cracks propagated gradually. Some materials with low strength first failed and promoted the crack initiation, which yields the stress concentration in the specimen. Then, crack propagated in continues region due to stress concentration, and high temperature exacerbated this process.

4.3 Strain rate

The axial steady-creep rates calculated from the secondary creep stage under various loadings are recognized and presented in Table 3 and Fig. 11(a). The rate plotted on semi-log axes was sensitive to the constant stress, showing an increasing trend. The axial steady-creep rates before creep failure were small and linearly increased with increasing constant stress but considerable augment can be observed when the final stresses were applied. Furthermore, under same stress levels, the secondary creep strain rate after high temperature treating was higher than that after lower temperature treating, especially, the rate of the

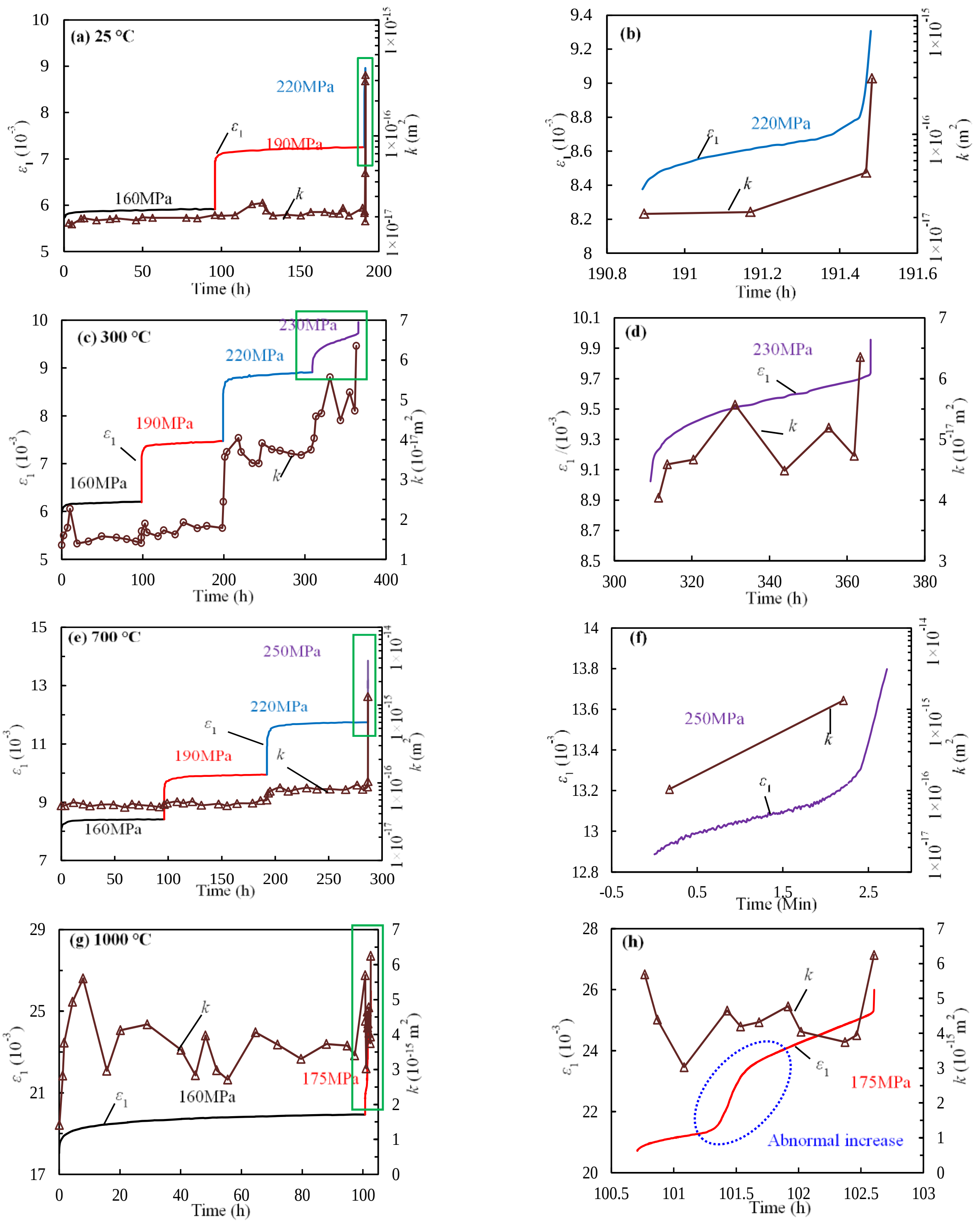

Fig. 10 Time-axial strain-permeability response of sandstone under different TID levels

1000°C specimen was approximately one order of magnitude larger than that of the other specimens before creep failure. The axial steady creep rates increased approximately 1-4 orders of magnitude subjected to the creep failure stresses. Figs. 11(a)-11(h) present the variation in strain rate as time went by. The strain rates plotted in log scale decreased gradually with increasing time at primary creep stage under low-stress levels. Under creep failure stresses, strain rates decreased gradually until constants with increasing time and remained unchanged during the secondary creep stage. Finally, tertiary creep occurred and strain rates increased in a short time.

The creep rate increased suddenly representing a failure for brittle sandstone (Xu and Yang 2016). The strain rates under creep failure stresses were also larger 1-4 orders of magnitude than that at low-stress levels. For the 1000°C sample, it seems to exhibit two three-stage creep curves. But creep failure did not occur for the former one. This may

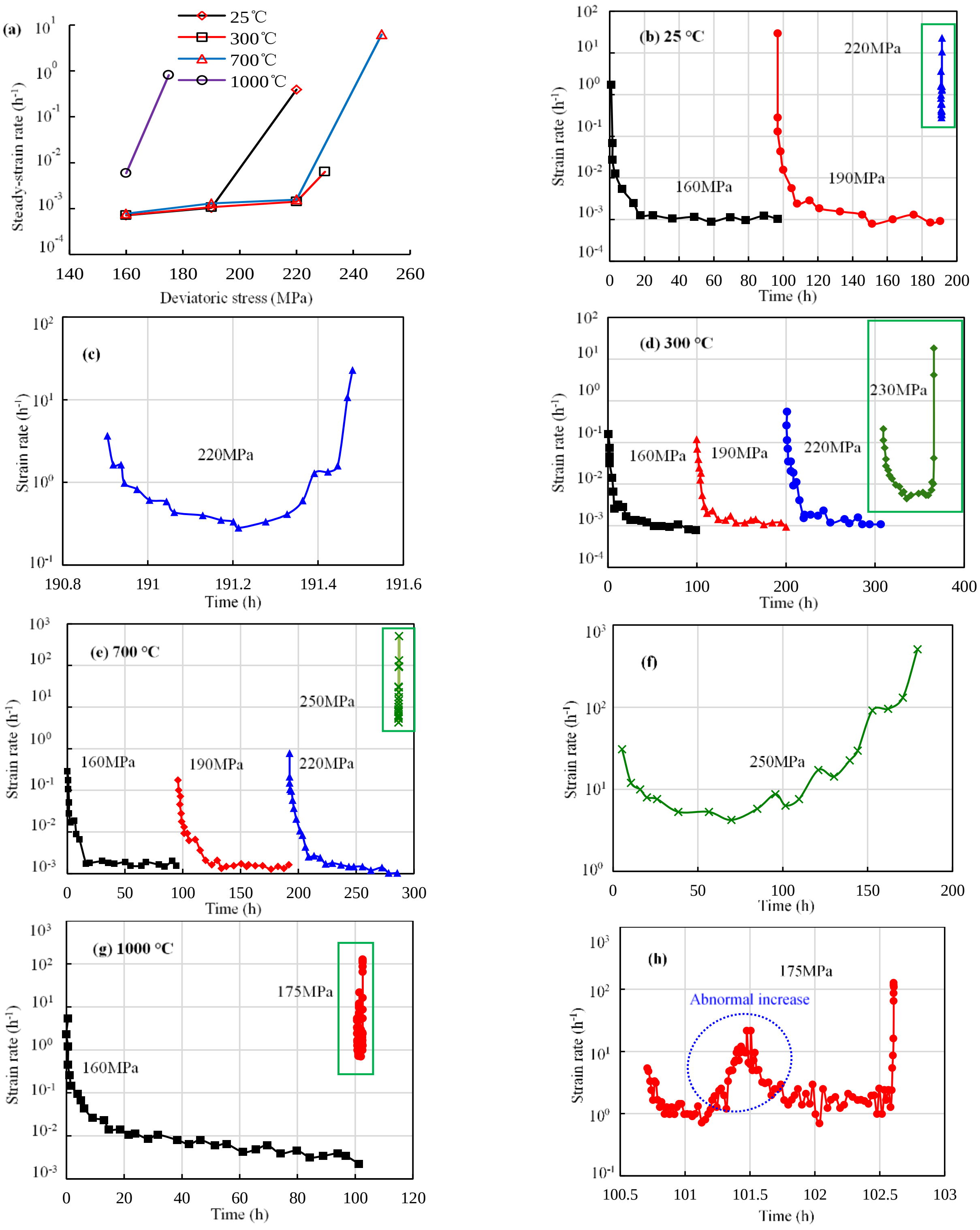

Fig. 11 Plot of strain rate vs. time of the specimen

be because the damage was generated within the sample which is not enough to induce creep failure.

4.4 Contrast failure pattern

Here, the rupture types of sandstones with different TID levels under conventional loading and constant loading are compared in Figs. 12(a) and (b). Under constant strain rate loading (see Fig. 12(a)), the failure mechanism of the sample was mixed tension and shear fracture except for the 1000°C specimen. The number of the lateral tensile crack increased, and the cracks moved toward central location with increasing temperature also excluding the 1000°C specimen. Main shear flaw and an obscure axial shear crack appeared in the specimen after 900°C and 1000°C heating. Detailed microstructures were observed in terms of photomicrographs of the specimens. As temperature increased above 700°C, a secondary shear plane sub-

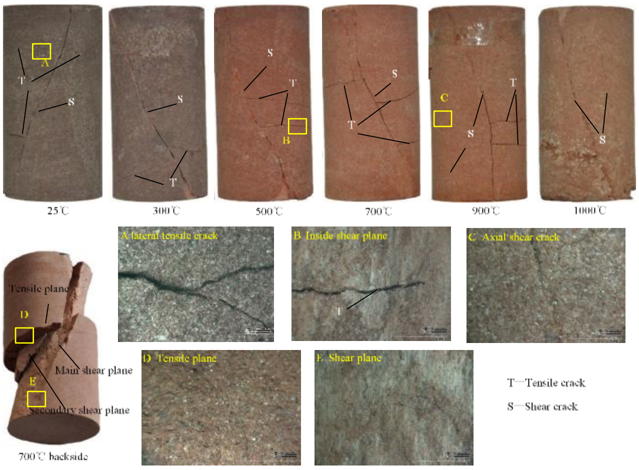

(a) Failure pattern of the samples under conventional loading

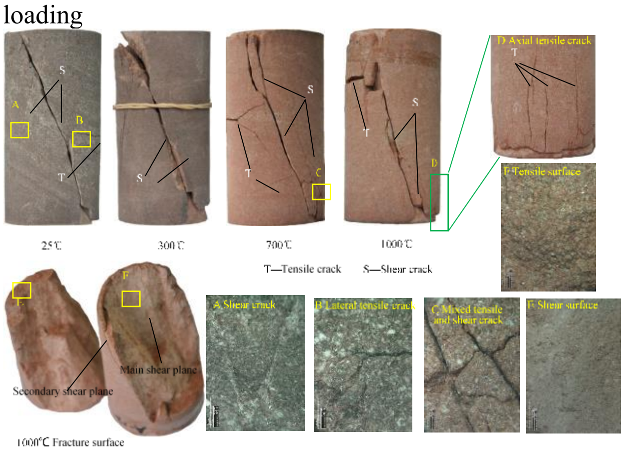

(b) Failure pattern of the samples under creep loading

Fig. 12 Plot of comparative failure modes of the specimens under two different loadings (*P*c=25MPa)

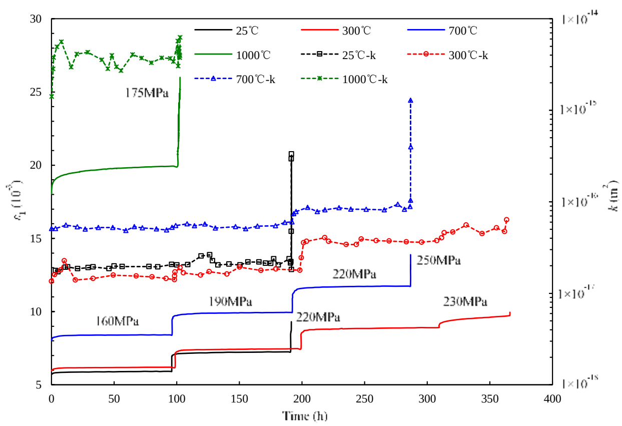

Fig. 13 Total permeability-time response of sandstone under different TID levels

parallel to the main shear plane appeared. In contrast, small particles on shear fractures gouge can be observed due to shear friction, whereas the tensile failure plane had no such particles (i.e., D and E position in the specimen).

As the TID level increased, the brittle property of rock deteriorated, but the ductility increased, the brittle-ductile transition occurred for the mineral grains. High-temperature damage generated thermal stress and yielded thermal cracks. Moreover, crystal plasticity of minerals became more evident and high-temperature induced chemical reactions. Therefore, rock deformation and failure mode transformed from brittle properties to plasticity flow (Gautam *et al*. 2016). The rupture type of sample became complicated due to the TID level increased. Increase in temperature resulted in specimens weakening of bonding among mineral grains, causing a decrease in tension strength (Liu *et al*. 2016), this can explain why the lateral tensile cracks move gradually from the two ends to the middle position of the specimens and then secondary axial shear plane appeared around the main shear crack. Lateral tensile cracks were dominated by the sliding of the secondary shear plane.

In contrast, under creep loadings, the specimens gave priority to shear destruction, and the tensile cracks appeared in the specimens (Fig. 12(b)). The 25 and 300°C specimens appeared shear failure, showing a similarly macro shear crack, respectively. In contrast, the 700 and 1000°C specimens failed in a complicated way; specifically, many shear sliding cracks grew around the main shear crack, and mixed tensile-shear cracks appeared in the 700°C specimen. A macro shear crack and an obscure secondary shear plane appeared in the 1000°C specimen. Besides, the lateral tensile cracks were induced by the secondary shear plane.This phenomenon is similar to the failure mode in the previous triaxial compressive experiments. An interesting phenomenon that visible axial tensile cracks governed by shear-slipping appeared at the local right side at the bottom of the 1000°C specimen. These phenomena indicated that the failure modes became complicated and the numbers of the shear and tensile crack increased with increasing temperature. A single macro shear crack and a secondary shear crack adjacent and parallel to the main shear crack appeared in the 700 and 1000°C specimens, whereas a single macro shear crack appeared on the rock surface below 700°C. There were many minor shear cracks parallel with the main shear crack and clusters of many minor axial tensile cracks on the right bottom regions in the 1000°C specimen under creep loading. This phenomenon was induced by the time-dependent slipping and dilation deformation.

4.5 Permeability evolution during creep process

The results of the axial deformation and variation of permeability during the creep process are shown in both Figs. 10 and 13, where the applied loadings in each step are also given. It is worth noting that the variations in permeability below 300°C were small, showing that the 25°C sample had a slightly large permeability compared to the 300°C sample. The permeability increased approximately two orders of magnitude until the TID level-up to 1000°C. As reported in Section 3.2, the effective porosity of the specimen was sensitive to the TID. The permeability of rock was highly dependent on rock microstructure and effective porosity. Mineral grains thermally expanded when temperature raised to 300°C, which induces micro-fissures and pores closure and to make sample became denser, narrowing the seepage networks for gas permeation. As a result, the effective porosity decreased slightly decreasing the permeability. When the temperature increased to 700°C, some minerals had been decomposed (Somerton 1992; Hajpál 2002), boundary cracks and micro-cracks generated by thermal stress in grains appeared. This thermal damage increased the effective porosity of rock and induced a considerable permeability to augment. Substantial damage cracks were induced when the TID level reached to 1000. The high-temperature effect further separated some grains from the sandstones matrix, amplifying the distance between grains and increasing the permeability by approximately two orders of magnitude. However, the sample heterogeneity also may induce that the porosity of the 25°C sample had slight larger porosity than that of the 300°C one. The difference in permeability between 25 and 300°C was so small that it is difficult to distinguish whether temperature effect or heterogeneity effect is the main reason. In the future, we will conduct more tests to further investigate this problem.

Besides, deviatoric stress also affects the permeability of the specimen. From Figs. 10 and 13 the permeability of the specimen under high-stress level is slightly higher than that at low-stress levels. The permeability has a sudden rise under creep failure stress. Moreover, the variations in the permeability of the specimens are complicated during the creeping stage. At the attenuation and secondary creep phase, the variations in the permeability of each rock show a similar evolution trend, first increasing gradually and then decreasing to a relatively steady state. There is no noticeable variation in the permeability of the specimen at the steady creep phase. Finally, the gas permeability curve takes a sudden rise during the tertiary rheology phase, in which the permeability increases approximately one order of magnitude and is higher than that under low stresses except for the 1000°C specimen. It is unfortunate that not enough data could be captured because creep fails in a very short time using the transient pulse decay method.

5. Conclusions

To explore the changes of physical features and creep-permeability behavior of sandstone on action of thermal damage, conventional triaxial compression and creep-permeability tests at 25 MPa confinement were performed on the sandstones after various TID levels heating.

• The effective porosity and permeability of the sample have no visible changes below 300°C, but they increased notably beyond 300°C due to the thermally-induced cracks increase the seepage channels. Finally, the 1000°C sample had nearly twice orders of magnitude as that at room temperature. The relationships between the normalized mass, volume and temperature can be divided into two linear stages: 25-700°C and beyond 700°C, showing a decrease of 1.8% in mass and an increase of 7% in volume from 25 to 1000°C. Moreover, the creep deformation also affected the permeability, showing an increasing trend during the primary creep stage and then decreasing to relative stabilization during the steady-state creep stage, subsequently, substantially increasing at the tertiary stage.

• There is no apparent compaction stage when the temperature was below 500°C, but the densification stage became obvious as temperature increased beyond 700°C, which can be divided into two phases: 25-500°C and beyond 700°C. The σ_p and σ_{cd} showed positive correlations with the TID levels (≤700°C) and then they were deteriorated by the TID beyond 700°C but the ε_{1p} and ε_{cd} continually increased with increasing the TID level. The E showed a small change below 300°C but been deteriorated by the TID subsequently.

• The creep deformation and the axial steady-creep rate were highly dependent on the loading and temperature. The specimens exhibited trimodal creep behaviors under the creep failure stresses. Tertiary creep was unable to be observed under relative low-stress levels. The axial deformations of the 300, 700 and 1000°C specimens were approximately 1.05, 1.4 and 3.1 times that of the 25°C specimen, respectively. The axial steady creep rates of the specimens before failure increased linearly with deviatoric stress, and the strain rates under creep failure stresses were larger 1-4 orders of magnitude than that at low-stress levels

• The failure modes of the specimens became more complex, and the numbers of the shear and tensile cracks increased with increasing the TID. Until the TID level raised above 700°C, a new shear plane sub-parallel to the main shear plane appeared, inducing lateral tensile cracks. In addition, creep deformation produced many shear sliding flaws to appear adjacent to the main shear crack during creep failure process

Acknowledgements

The research described in this paper was financially supported by the Fundamental Research Funds for the Central Universities (2018BSCXC38) and Postgraduate Research & Practice Innovation Program of Jiangsu Province (KYCX18_1976).

References

Brace, W.F., Walsh, J.B. and Frangos, W.T. (1968), “Permeability of granite under high pressure”, *J. Geophys. Res.*, **73**(6), 2225-2236. https://doi.org/10.1029/JB073i006p02225.

Chen, G.Q., Li, T.B., Wang, W., Guo F. and Yin HY. (2017a), “Characterization of the brittleness of hard rock at different temperatures using uniaxial compression tests”, *Geomech. Eng.*, **13**(1), 63-77. https://doi.org/10.12989/gae.2017.13.1.063

Chen, L., Wang, P., Liu, J.F., Li, Y., Liu, J. and Wang, J. (2017b), “Effects of temperature and stress on the time-dependent behavior of Beishan granite”, *Int. J. Rock Mech. Min. Sci.*, **93**, 316-323. https://doi.org/10.1016/j.ijrmms.2016.11.007.

Chopra, P.N. (1997), “High-temperature transient creep in olivine rocks”, *Tectonophysics*, **279**(1-4), 93-111. https://doi.org/10.1016/S0040-1951(97)00134-0.

David, C., Menéndez, B. and Darot, M. (1999), “Influence of stress-induced and thermal cracking on physical properties and microstructure of la peyratte granite” *Int. J. Rock Mech. Min. Sci.*, **36**(4), 433-448. https://doi.org/10.1016/S0148-9062(99)00010-8.

Dragon, A. and Mroz, Z.A. (1978), “Continuum model for plastic-brittle behaviour of rock and concrete”, *Int. J. Eng. Sci.*, **17**(2), 121-137. https://doi.org/10.1016/0020-7225(79)90058-2.

Gautam, P.K., Verma, A.K., Jha, M.K., Sarkar, K., Singh, T.N. and Bajpai, R.K. (2016), "Study of strain rate and thermal damage of Dholpur sandstone at elevated temperature", *Rock Mech. Rock Eng.*, **49**(9), 1-11. https://doi.org/10.1007/s00603-016-0965-5.

Géraud, Y. (1994) "Variations of connected porosity and inferred permeability in a thermally cracked granite", *Geophys. Res. Lett.*, **21**(11), 979-982. https://doi.org/10.1029/94GL00642.

Glover, P.W.J., Baud, P., Darot, M., Meredith, P.G., Boon, S.A., LeRevelec, M., Zoussi, S. and Reuschle, T. (1995), "α/β phase transition in quartz monitored using acoustic emissions", *Geophys. J. Int.*, **120**(3), 775-782. https://doi.org/10.1111/j.1365-246X.1995.tb01852.x.

Hajpál, M. (2002), "Changes in sandstones of historical Monuments Exposed to fire or high temperature", *Fire Technol.*, **38**(4), 373-382. https://doi.org/10.1023/A:102017450.

Hajpál, M. and Török, Á. (1989), "Petrophysical and mineralogical studies of burnt sandstones", *Proceedings of the 2nd International PhD Symposium in Civil Engineering*, Budapest, Hungary.

Hajpál, M. and Török, Á. (2004), "Mineralogical and colour changes of quartz sandstones by heat", *Environ. Geol.*, **46**(3-4), 311-322. https://doi.org/10.1007/s00254-004-1034-z.

Heap, M.J., Baud, P. and Meredith, P.G. (2009), "Influence of temperature on brittle creep in sandstones", *Geophys. Res. Lett.*, **36**(19), L19305. https://doi.org/10.1029/2009GL039373.

Heuze, F.E. (1983), "High-temperature mechanical, physical and thermal properties of granitic rocks-a review", *Int. J. Rock Mech. Min. Sci. Geomech. Abstr.*, **20**(1), 3-10. https://doi.org/10.1016/0148-9062(83)91609-1.

Huang, Y.H., Yang, S.Q., Tian, W.L., Zhao, J., Ma, D. and Zhang, C.S. (2017), "Physical and mechanical behavior of granite containing pre-existing holes after high temperature treatment", *Arch. Civ. Mech. Eng.*, **17**(4), 912-925. https://doi.org/10.1016/j.acme.2017.03.007.

Hudson, J.A., Stephansson, O. and Andersson, J. (2005), "Guidance on numerical modeling of thermo-hydro-mechanical coupled processes for performance assessment of radioactive waste repositories", *Int. J. Rock Mech. Min. Sci.*, **42**(5-6), 850-870. https://doi.org/10.1016/j.ijrmms.2005.03.018.

ISRM (2007), *The Complete ISRM Suggested Methods for Rock Characterization, Testing and Monitoring: 1974-2006. Suggested Methods Prepared by the Commission on Testing Methods*, International Society for Rock Mechanics, Compilation Arranged by the ISRM Turkish National Group, Ankara, Turkey.

Kong, B., Wang, E.Y., Li, Z.H., Wong, X.R., Liu, X.F., Li, N. and Yang, Y.L. (2016), "Electromagnetic radiation characteristics and mechanical properties of deformed and fractured sandstone after high temperature treatment", *Eng. Geol.*, **209**, 82-92. https://doi.org/10.1016/j.enggeo.2016.05.009.

Kumari, W.G.P., Ranjith, P.G., Perera, M.S.A., Shao, S., Chen, B.K., Lashin, A.A.I, Arifi, N. and Rathnaweera, T.D. (2017), "Mechanical behaviour of Australian Strathbogie granite under in-situ stress and temperature conditions: An application to geothermal energy extraction", *Geothermics*, **65**, 44-59. https://doi.org/10.1016/j.geothermics.2016.07.002.

Lan, J.L. (2009), "A study of the mechanical properties of sandstone after cyclic thermal action", M.Sc. Dissertation, National Cheng Kung University, Taiwan.

Liu, X., Yuan, S., Sieffert, Y., Fityus, S. and Buzzi, O. (2016), "Changes in mineralogy, microstructure, compressive strength and intrinsic permeability of two sedimentary rocks subjected to high-temperature heating", *Rock Mech. Rock Eng.*, **49**(8), 2985-2998. https://doi.org/10.1007/s00603-016-0950-z.

Lü, C., Sun, Q., Zhang, W.Q., Geng, J.S., Qi, Y.M. and Lu, L.L. (2017), "The effect of high temperature on tensile strength of sandstone", *Appl. Thermal Eng.*, **111**, 573-579. https://doi.org/10.1016/j.applthermaleng.2016.09.151.

Luo, J. and Wang, L. (2011), "High-temperature mechanical properties of mudstone in the process of underground coal gasification", *Rock Mech. Rock Eng.*, **44**(6), 749. https://doi.org/10.1007/s00603-011-0168-z.

Lyons, K.D., Honeygan, S. and Moroz, T. (2007), "NETL extreme drilling laboratory studies high pressure high temperature drilling phenomena", *J. Energy Resour. Technol.*, **130**(4), 791-796. https://doi.org/10.1115/1.3000139.

Minchener, A.J. (2005), "Coal gasification for advanced power generation", *Fuel*, **84**(17), 2222-2235. https://doi.org/10.1016/j.fuel.2005.08.035.

Miura, K., Okui, Y. and Horii, H. (2003), "Micromechanics-based prediction of creep failure of hard rock for long-term safety of high-level radioactive waste disposal system", *Mech. Mater.*, **35**(3), 587-601. https://doi.org/10.1016/S0167-6636(02)00286-7.

Moradi, S.S.T., Nikolaev, N.I., Chudinova, I.V. and Martel A.S. (2018), "Geomechanical study of well stability in high-pressure, high-temperature conditions", *Geomech. Eng.*, **16**(3), 331-339. http://dx.doi.org/10.12989/gae.2018.16.3.331.

Otto, C. and Kempka, T. (2015), "Thermo-mechanical simulations of rock behavior in underground coal gasification show negligible impact of temperature-dependent parameters on permeability changes", *Energies*, **8**(6), 5800-5827. https://doi.org/10.3390/en8065800.

Ranjith, P.G., Daniel, R.V., Chen, B.J. and Perera, M.S.A. (2012), "Transformation plasticity and the effect of temperature on the mechanical behaviour of Hawkesbury sandstone at atmospheric pressure", *Eng. Geol.*, **151**, 120-127. https://doi.org/10.1016/j.enggeo.2012.09.007.

Scott, T.E. and Nielsen, K.C. (1991), "The effects of porosity on the brittle-ductile transition in sandstones", *J. Geophys. Res.*, **96** (B1), 405-414. https://doi.org/10.1029/90JB02069.

Shafiei, A. and Dusseault, M.B. (2013), "Geomechanics of thermal viscous oil production in sandstones", *J. Petrol. Sci. Eng.*, **103**(3), 121-139. https://doi.org/10.1016/j.petrol.2013.02.001.

Sirdesai, N.N., Singh, T.N., Ranjith, P.G. and Singh, R. (2017), "Effect of varied durations of thermal treatment on the tensile strength of red sandstone", *Rock Mech. Rock Eng.*, **50**(1), 1-9. https://doi.org/10.1007/s00603-016-1047-4.

Somerton, W.H. (1992), *Thermal Properties and Temperature-related Behavior of Rock/Fluid Systems*, Elsevier, Amsterdam, The Netherlands, 22-29.

Sun, H., Sun, Q., Deng, W., Zhang, W. and Chao, L. (2017), "Temperature effect on microstructure and p-wave propagation in Linyi sandstone", *Appl. Thermal Eng.*, **115**, 913-922. https://doi.org/10.1016/j.applthermaleng.2017.01.026.

Sun, Q., Lü, C., Cao, L.W., Li, W.C., Geng, J.S. and Zhang, W.Q. (2016), "Thermal properties of sandstone after treatment at high temperature", *Int. J. Rock Mech. Min. Sci.*, **85**, 60-66. https://doi.org/10.1016/j.ijrmms.2016.03.006.

Tang, F.R., Wang, L.G., Lu, Y.L. and Yang, X.Q. (2015), "Thermophysical properties of coal measure strata under high temperature", *Environ. Earth Sci.*, **73**(10), 6009-6018. https://doi.org/10.1007/s12665-015-4364-0.

The National Standards Compilation Group of People Republic's China. (2009), *Methods for Determining the Physical and Mechanical Properties of Coal and Rock-Part 4: Methods for Calculating the Porosity of Coal and Rock (GB/T23561.4)*, China Planning Press, Beijing, China (in Chinese).

Tian, H., Kempka, T., Xu, N.X. and Ziegle, M. (2012), "Physical properties of sandstones after high temperature treatment", *Rock Mech. Rock Eng.*, **45**(6), 1113-1117. https://doi.org/10.1007/s00603-012-0228-z.

Tiskatine, R., Eddemani, A., Gourdo, L., Abnay, B., Ihlal, A., Aharoune, A. and Bouirden, L. (2016), “Experimental evaluation of thermo-mechanical performances of candidate rocks for use in high temperature thermal storage”, *Appl. Energy*, **171**, 243-255. https://doi.org/10.1016/j.apenergy.2016.03.061.

Uribe-Patiño, J.A., Alzate-Espinosa, G.A. and Arbeláez-Londoño, A. (2017), “Geomechanical aspects of reservoir thermal alteration: A literature review”, *J. Petrol. Sci. Eng.*, **152**, 250-266. https://doi.org/10.1016/j.petrol.2017.03.012.

Wu, Q.H., Weng, L., Zhao, Y.L., Guo B.H. and Tao L. (2019), “On the tensile mechanical characteristics of fine-grained granite after heating/cooling treatments with different cooling rates”, *Eng. Geol.*, **253**, 94-110. https://doi.org/10.1016/j.enggeo.2019.03.014.

Wu, Z., Qin, B.D., Chen, L.J. and Luo, Y.Y. (2005), “Experimental study on mechanical character of sandstone of the upper plank of coal bed under high temperature”, *Chin. J. Rock Mech. Eng.*, **24**(11), 1863-1867 (in Chinese).

Xu, P. and Yang, S.Q. (2016), “Permeability evolution of sandstone under short-term and long-term triaxial compression”, *Int. J. Rock Mech. Min. Sci.*, **85**, 152-164. https://doi.org/10.1016/j.ijrmms.2016.03.016.

Yang, S.Q., Hu, B., Ranjith, P. and Xu P. (2018a), “Multi-step loading creep behavior of red sandstone after thermal treatments and a creep damage model”, *Energies*, **11**(1), 212. https://doi.org/10.3390/en11010212.

Yang, S.Q. and Hu, B. (2018b), “Creep and long-term permeability of a red sandstone subjected to cyclic loading after thermal treatments”, *Rock Mech. Rock Eng.*, **51**(10), 2981-3004. https://doi.org/10.1007/s00603-018-1528-8.

Yang, S.Q., Jing, H.W. and Cheng, L. (2014), “Influences of pore pressure on short-term and creep mechanical behavior of red sandstone”, *Eng. Geol.*, **179**, 10-23. https://doi.org/10.1016/j.enggeo.2014.06.016.

Yang, S.Q., Xu, P., Li, Y.B. and Huang, Y.H. (2017), “Experimental investigation on triaxial mechanical and permeability behavior of sandstone after exposure to different high temperature treatments”, *Geothermics*, **69**, 93-109. https://doi.org/10.1016/j.geothermics.2017.04.009.

Ye, G.L., Nishimura, T. and Zhang, F. (2015), “Experimental study on shear and creep behaviour of green tuff at high temperatures”, *Int. J. Rock Mech. Min. Sci.*, **79**, 19-28. https://doi.org/10.1016/j.ijrmms.2015.08.005.

Zhang, P., Mishra, B. and Heasley, K.A. (2015), “Experimental investigation on the influence of high pressure and high temperature on the mechanical properties of deep reservoir rocks”, *Rock Mech. Rock Eng.*, **48**(6), 2197-2211. https://doi.org/10.1007/s00603-015-0718-x.

Zhang, W., Sun, Q., Hao, S., Geng, J. and Lv, C. (2016), “Experimental study on the variation of physical and mechanical properties of rock after high temperature treatment”, *Appl. Thermal Eng.*, **98**, 1297-1304. https://doi.org/10.1016/j.applthermaleng.2016.01.010.

CC